Distributed Injection-Locked Frequency Dividers

Alireza Imani and Hossein Hashemi, *Senior Member, IEEE*

Abstract—**Distributed injection-locked frequency division is introduced as a method to increase the locking range beyond that of conventional injection-locked frequency dividers. It is analytically shown that continuous frequency division can be achieved over a frequency range that spans over multiples of the self-oscillation frequency of the core divider. Design techniques in millimeter-waves are discussed in detail. A proof-of-concept prototype, realized in a foundry 130-nm BiCMOS SiGe HBT technology, achieves a measured locking range of 35–44 and 41–59.5 GHz while consuming 3.8 mW from a 1.15-V supply.**

Index Terms—**Distributed, frequency divider, frequency synthesis, injection locking, injection-locked frequency divider, millimeter wave (mm-wave), phase locked loop.**

I. INTRODUCTION

AMONG different topologies, latch-based frequency dividers have the widest locking range and fully leverage the advantages of technology scaling [7]. However, for each technology node, there is a higher bound on their maximum operation frequency, which is significantly lower than the maximum oscillation frequency of the devices in that technology. This limit in higher frequency operation can be bridged by using injection-locked frequency dividers; but, a conventional design will result in a limited frequency locking range. Different techniques have been explored to improve the locking range of the injection-locked dividers [2], [4], [5]. These techniques generally aim at improving the injection efficiency over wider range of frequencies using passive structures. For example, a passive *LC* circuit may be added between the injection device and the active core to track the impedance of the tank and improve the injection strength over a wider range of frequencies [2]. Here, we propose a very effective method in achieving wideband injection-locked dividers. In the proposed solution, named distributed injection-locked frequency division, the injection device is broken down to several smaller devices. These multiple injection devices sit at different nodes of an *LC*-ladder network. As analytically and experimentally verified in this paper, this enables wideband frequency locking. If designed properly, the injection-locked frequency divider can operate over multiples of its first resonance frequency.

To the best of our knowledge, this property has not been shown in any other injection-locked frequency divider.

A. Imani is with Broadcom Limited, Irvine, CA 92617 USA (e-mail: alireza.imani@broadcom.com).

H. Hashemi is with the Department of Electrical Engineering Electrophysics, University of Southern California, Los Angeles, CA 90089 USA (e-mail: hosseinh@usc.edu).
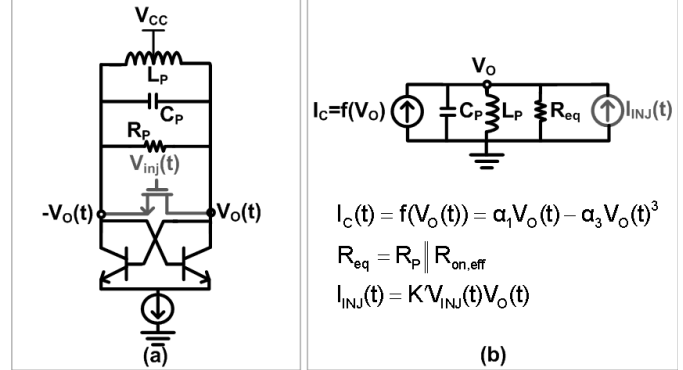
Fig. 1. (a) Conventional injection-locked frequency divider and (b) its first-order model where the injection device is assumed to be always ON.

Section II is dedicated to analysis, simulation, and comparison of the conventional injection-locked frequency divider and distributed injection-locked frequency divider. Section III details the prototype implementation, measurements, and comparison to simulations and state of the art. Section IV concludes this paper.

II. ANALYSIS OF DISTRIBUTED INJECTION-LOCKED DIVIDER

A. Conventional Injection-Locked Frequency Divider

In a conventional injection-locked frequency divider, as shown in Fig. 1(a), a signal is injected at a frequency close to twice the frequency of the *LC* resonant tank. Throughout this paper, bipolar symbol is used for the core transistors, and FET symbol is used for the injection switch. This ensures consistency with the experimental prototypes; however, the underlying analysis and results are independent of transistor types. A simplified model of the conventional injection-locked frequency divider is shown in Fig. 1(b). The cross-coupled pair is modeled as a current source with a third-order polynomial dependence to the voltage across it, where $\alpha_1 > 0$ and $\alpha_3 > 0$ are determined by the tail dc current and core devices. The injection device (FET) is modeled with an effective ON resistance, $R_{\text{on,eff}}$, and a mixing injection current, $I_{\text{inj}}(t)$. Referring to Appendix A, this model is valid if the injection device is always ON during the operation of the injection-locked frequency divider.

Differential equations for amplitude and phase of the output voltage $V_O(t)$ can be formed using the averaging technique [8] and assuming

$$
\begin{cases}
V_O(t) = V_{\text{CC}} + a(t)\cos(\underbrace{\omega_0 t + \phi(t)}_{\Theta_o}), \\
\omega_0 = \frac{1}{\sqrt{L_P C_P}} \\
V_{\text{inj}}(t) = V_G + V_{\text{inj}}\cos(\underbrace{\omega_{\text{inj}}t}_{\Theta_{\text{inj}}}), \\
\omega_{\text{inj}} = 2\omega_0 + 2\Delta\omega
\end{cases}
\tag{1}
$$

and can be written as

$$
\begin{cases}
\frac{da(t)}{dt} = \left(\frac{\alpha_1 - \frac{1}{R_{eq}}}{2C}\right) a(t) - \frac{3\alpha_3}{8C} a(t)^3 \\
\qquad + a(t) \frac{K'V_{inj}}{2} \cos(2\phi(t) - 2\Delta\omega t) \\
\frac{d\phi(t)}{dt} = \frac{K'V_{inj}}{C} \sin(2\phi(t) - 2\Delta\omega t)
\end{cases}
\tag{2}
$$

where K' is defined in Appendix A. Under locked condition, the oscillation frequency will be equal to half the injection frequency ($\omega_{inj}/2 = \omega_0 + \Delta\omega$). Therefore, $\phi(t) = \Delta\omega t + \chi$, where χ is the phase difference between input and locked output waveforms. Applying this condition to the phase differential equation results in

$$
\Delta\omega = \frac{K'V_{inj}}{C} \sin(2\chi).
\tag{3}
$$

The locking range is given by $\Delta\omega < ((K'V_{inj})/(C))$ and $\chi = \pm\pi/4$ at the edges of locking range. This requirement is typically referred to as the "phase condition" and is analogous to the Adler expression for injection-locked oscillators [9]. According to this condition, increasing the size of the injection device (K') and the amplitude of the injection signal (V_{inj}) should increase the locking range. Under the locked condition, the amplitude differential equation simplifies to

$$
\frac{da(t)}{dt} = \frac{1}{2C}\left(\alpha_1 - \frac{1}{R_{eq}} + \frac{K'V_{inj}}{2}\cos(2\chi)\right) a(t) - \frac{3\alpha_3}{8C} a(t)^3.
\tag{4}
$$

For the amplitude differential equation to have a nonzero stable point, we need to have $\alpha_1 - ((1)/(R_{eq})) + ((K'V_{inj})/2)\cos(2\chi) > 0$. Within the locking range, $|\chi| < ((\pi)/(4))$ and $0 < \cos(2\chi) < 1$. If $\alpha_1 - ((1)/(R_{eq}))$ is larger than zero, i.e., the divider starts self-oscillations without injection, this condition is always satisfied and the locking range will be determined by the phase condition of (3). Without self-oscillation, if $\alpha_1 - (1/(R_{eq}) + ((K'V_{inj})/(2)) > 0$, then the amplitude equation will have a nonzero stable point, and the locking range will be determined by

$$
\alpha_1 - \frac{1}{R_{eq}} + K'V_{inj}\cos(2\chi) = 0
\tag{5}
$$

where according to (3), $\cos(2\chi) = (1 - ((C\Delta\omega)/(K'V_{inj}))^2)^{1/2}$. This condition is referred to as the "gain condition."

In the conclusion, if the switch is ON during the entire operation cycle, the frequency divider operates at two separate regimes.

1) If self-oscillation occurs, the locking range is determined by the phase condition given by (3). In this regime, the divider output will show frequency pulling behavior outside of the locking range.
2) If self-oscillation does not occur, enough injection strength can result in frequency division as predicted by (5). In this regime, the divider output will be zero outside the locking range.

Fig. 2(a) and (b) shows the sensitivity curves obtained from simulation and analysis of the model shown in Fig. 1(b) and the schematic shown in Fig. 1(a) in these two regions.
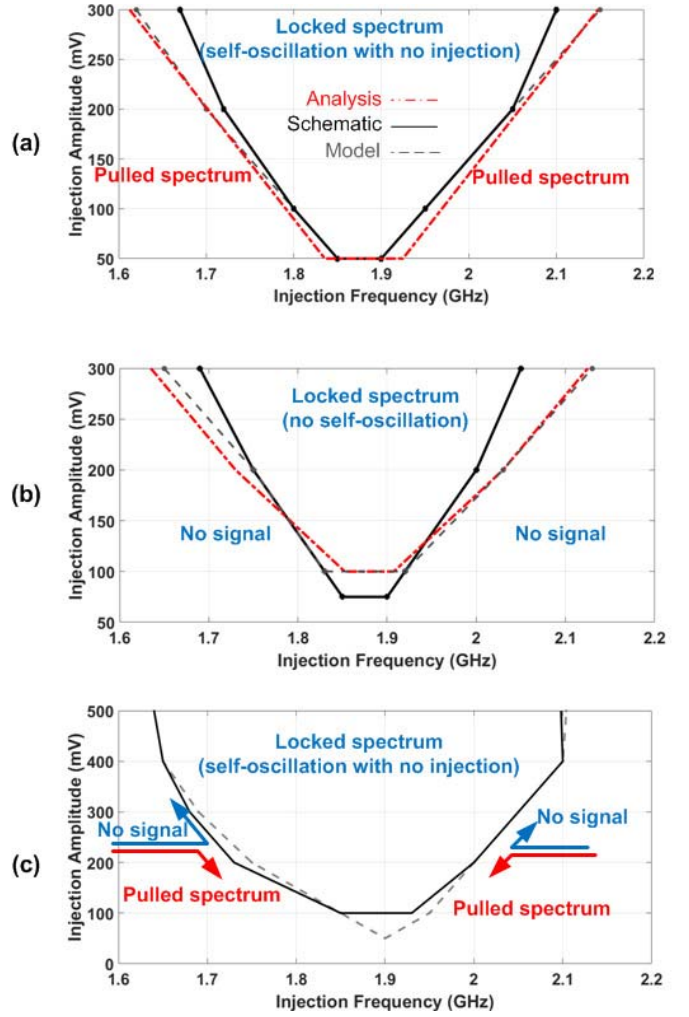

Fig. 2. Different regimes in the conventional injection-locked frequency divider. (a) Switch always ON and self-oscillation occurs ($I_{dc} = 820\,\mu A$, $V_{GATE} = 1.7$ V, $W = 6\,\mu m$, $V_{CC} = 1.1$ V, $R_{ON} = 120\,\Omega$, $\alpha_1 = 14.6$ mA/V, $\alpha_3 = 1\,A/V^3$, and $K' = 0.037\,A/v^2$). (b) Switch always ON and no self-oscillation ($I_{dc} = 410\,\mu A$, $V_{GATE} = 1.7$ V, $W = 6\,\mu m$, $V_{CC} = 1.1$ V, $R_{ON} = 120\,\Omega$, $\alpha_1 = 7.3\,mA/V$, $\alpha_3 = 0.5\,A/V^3$, and $K' = 0.037\,A/v^2$). (c) Switch biased at verge of being ON and self-oscillation happens ($I_{dc} = 300\,\mu A$, $V_{GATE} = 1.4$ V, $W = 6\,\mu m$, $V_{CC} = 1.1$ V, $R_{ON} = 1000\,\Omega$, and $\alpha_1 = 5.5$ mA/V).

It is verified that based on this model, the injection-locked frequency divider will only operate in these two regimes.

If the injection device is not ON at all times, its current needs to be modified according to (22), and the injection-locked frequency divider can have other operation regimes. As an example, consider the scenario where the injection device is biased at the verge of being ON ($V_G - V_{CC} = V_{th}$) and $a(t) << V_{INJ}$. According to (22), the switch current can then be approximately written as

$$
I_{SW} = \begin{cases}
0, & \cos\Theta_{inj} < 0 \\
2K'V_{inj}V_o\cos\Theta_{inj}\cos\Theta_o & \text{otherwise}
\end{cases}
$$
$$
= 2K'V_{inj}V_o\cos\Theta_{inj}\cos\Theta_o(1/2 + S_{1/2}(\Theta_{inj}))
\tag{6}
$$

where $S_{1/2}(.)$ is a half-amplitude square-wave signal. The averaged differential equation for amplitude can now be

formed as

$$\frac{da(t)}{dt} = \frac{1}{2C}\left(\alpha_1 - \frac{1}{R_{\text{eq}}} + \frac{K'V_{\text{inj}}(2\cos(2\chi) - \pi)}{4}\right)a(t)$$
$$- \frac{3\alpha_3}{8C}a(t)^3. \tag{7}$$

In this case, the "gain condition" can be written as $\alpha_1 - ((1)/(R_P)) + ((K'V_{\text{inj}}(2\cos(2\chi) - \pi))/(4)) > 0$. In this scenario, even if self-oscillations exist $\alpha_1 - ((1)/(R_P)) > 0$ and phase condition is satisfied, the divider can lose lock at the edges if gain condition is not satisfied. Fig. 2(c) shows the schematic and model simulations in this scenario. It is observed both from schematic and model simulations, that unlike previous scenario, injection signal only exacerbates the gain condition. Furthermore, as predicted by (7), it is observed that for increased injection strength, the gain condition becomes dominant and the divider output dies down at the edges of the locking range instead of showing frequency pulling behavior.

B. Distributed Injection-Locked Frequency Divider

The locking range of a conventional injection-locked frequency divider depends on the injection power (V_{inj}), size of the injection device (K'), quality factor of the tank (R_{eq} and C), and the active core (α_1). On the one hand, larger injection device size and input power are desirable to increase the strength of the injected signal (enhanced phase condition). On the other hand, larger size of the injection device increases its conductance, which can stop the output from oscillation (reduced gain condition). Larger injection device size also increases the parasitic capacitance at the tank nodes resulting in lower maximum frequency and/or higher power consumption (smaller inductor and higher power). Lower quality factor tank generally increases the locking range; but, necessitates increased power consumption to satisfy the gain condition.

Fig. 3 shows a schematic of the proposed distributed injection-locked frequency divider. In this scheme, the injection device is broken down to multiple smaller injection devices. As it will be discussed in this section, this can yield significant increase in the locking range. To start the analysis, consider the N-element and infinitely long LC-ladders shown in Fig. 4. Parallel capacitors represent the parasitics of the distributed injection devices. The ladder exhibits several series and parallel mode resonances. Steady-state equations for the infinitely long ladder can be written as

$$\begin{cases} I_{k+1} - I_k = -C_1 j\omega V_k, \\ V_m = -L_1 j\omega \sum_{k=1}^{m} I_k. \end{cases} \tag{8}$$

From these equations, one can find the difference equation for ladder currents. The difference equation may be analyzed by taking the one-sided z-transform of the equation to find all the currents as a function of I_1 (Appendix B). This will lead to

$$\begin{cases} I_n \approx I_1(1 - \alpha/2)^{n-1}\cos(\sqrt{\alpha}(n-1)) \\ \quad \approx I_1\cos(\sqrt{\alpha}(n-1)) \\ V_n \approx -jZ_0 I_1 \sin(\sqrt{\alpha}n) \end{cases} \tag{9}$$
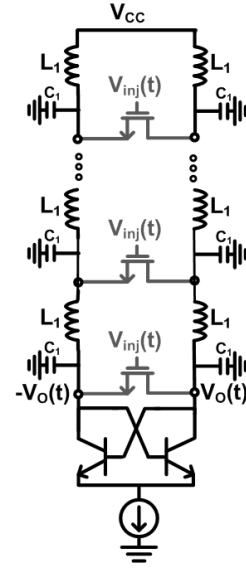

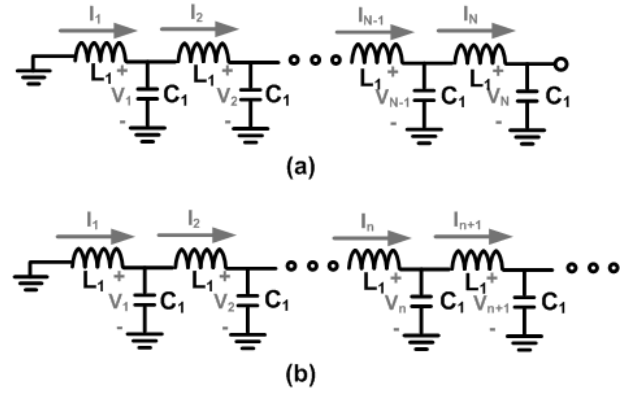Fig. 3. Schematic of the proposed distributed injection-locked frequency divider.

Fig. 4. (a) N-element LC-ladder. (b) One-sided infinitely long LC-ladder.

where $\alpha = L_1 C_1 \omega^2$ and $Z_0 = (L_1/C_1)^{1/2}$. The approximations hold as long as $\alpha n \ll 1$, which will prove to be valid for our region of interest as it will come clear shortly. Looking now into the N-element array, the parallel mode resonances happen when the current out of the ladder is zero independent of the network that it gets connected to. At this mode, the first N-elements of the infinite network and the N-element network will be equivalent since the dynamical equations are the same and the current out of the Nth node is 0. Therefore, the first parallel mode resonance frequency (ω_{1p}) of the N-element array can be found as

$$\cos(\sqrt{\alpha}N) = 0 \rightarrow \sqrt{\alpha}N = \pi/2 \rightarrow \omega_{1p} = \frac{\pi}{2N\sqrt{L_1 C_1}}. \tag{10}$$

With the same token, all parallel modes are the solutions of $\cos((\alpha)^{1/2}N) = 0$. In the series mode, the Nth node voltage will be zero and based on (9), they happen when $\sin((\alpha)^{1/2}N) = 0$. In summary, the parallel and series
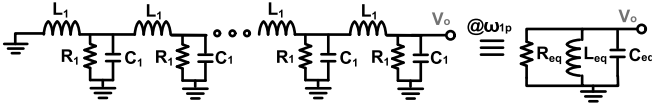
Fig. 5.   Equivalent circuit around the first parallel mode resonance.

resonances of the N-element LC-ladder can be given by

$$\begin{cases} \omega_{ip} = \dfrac{i\pi}{2N\sqrt{L_1 C_1}} \\ \omega_{is} = \dfrac{i\pi}{N\sqrt{L_1 C_1}}. \end{cases} \tag{11}$$

The N-element LC-ladder may be represented with an equivalent parallel (series) LC tank around its parallel (series) resonant frequencies [10]. To find the equivalent parallel tank of the network around its first parallel mode resonance (as shown in Fig. 5), we will equate the maximum capacitive energy stored in the two networks for the same voltage swing at the output node

$$1/2 C_{eq} V_o^2 = 1/2 C_1 \sum_{i=1}^{N} V_n^2 \approx 1/2 C_1 V_o^2 \sum_{i=1}^{N} \sin^2\left(\frac{\pi}{2N}i\right)$$

$$\Rightarrow C_{eq} = C_1 \sum_{i=1}^{N} \sin^2\left(\frac{\pi}{2N}i\right) \tag{12}$$

where the voltages across C_1 capacitors were replaced according to (9). As an example, for a ten-stage LC-ladder network, the first parallel mode equivalent capacitance is $C_{eq} = 5.5 C_1$. The equivalent inductance can readily be calculated from (10) and (11). In the distributed injection-locked frequency divider of Fig. 3, the loss is dominated by the ON resistance of the distributed injection devices, and may be represented with resistors R_1 in parallel with capacitors C_1 in the equivalent ladder networks of Fig. 4. An equivalent parallel resistance R_{eq} can be derived following a similar approach in deriving C_{eq} (Fig. 5). It can be shown that $Q = R_1 C_1 \omega_{1p} = R_{eq} C_{eq} \omega_{1p}$. Fig. 6 shows the schematic simulations of a ten-element ladder and its equivalent RLC tank at the first parallel resonance mode.

Now that we have found the open circuit impedance of the LC ladder, we will proceed to the equivalent short-circuit current (Norton equivalent) due to the distributed injection signals. Fig. 7(a) shows the N-element ladder. To analyze this circuit, consider the double-sided infinitely long LC ladder shown in Fig. 7(b). The currents and voltages at node n of the infinite ladder due to the injection signal $I_{inj,p}$ can be calculated using the double-sided z-transform and may be written as

$$\begin{cases} I_n \approx \dfrac{I_{inj,p}}{2} \cos(\sqrt{\alpha}(n-p)) \\ V_n \approx -j Z_0 \dfrac{I_{inj,p}}{2} \sin(\sqrt{\alpha}(n-p)). \end{cases} \tag{13}$$

To make the infinite-element ladder equivalent to the N-element ladder, we add two additional injection signals $I_{aux,1}$ and $I_{aux,N}$, as shown in Fig. 7, and use superposition to force nodes 1 and N in the infinitely long ladder to have 0 V (virtual ground). Based on (13), the values of the additional signals

need to be

$$\begin{cases} I_{aux,1} = -I_{inj,p} \dfrac{\sin(\sqrt{\alpha}(N-p))}{\sin(\sqrt{\alpha}N)} \\ I_{aux,N} = -I_{inj,p} \dfrac{\sin(\sqrt{\alpha}p)}{\sin(\sqrt{\alpha}N)}. \end{cases} \tag{14}$$

Using superposition, the short-circuit current due to the injection signal in the N-element LC-ladder can now be calculated as

$$\begin{aligned} I_{SC,p} \\ = \frac{I_{inj,p}}{2} \cos(\sqrt{\alpha}(N-p)) \\ + \frac{I_{inj,p}}{2} \frac{\sin(\sqrt{\alpha}p)\cos(\sqrt{\alpha}) - \cos(\sqrt{\alpha}N)\sin(\sqrt{\alpha}(N-p))}{\sin(\sqrt{\alpha}N)}. \end{aligned} \tag{15}$$

At the first parallel mode resonance frequency, i.e., $(\alpha)^{1/2} N = \pi/2$, (15) simplifies to

$$I_{SC,p}|_{@\,\omega_{1p}} = I_{inj,p} \sin(\sqrt{\alpha}p). \tag{16}$$

Going back to the injection-locked frequency divider schematics of Figs. 1(a) and 3, and according to Appendix A, the injection current by each injection device is a mixing product of the injected signal and the voltage swing at injection node. Therefore, since the voltages at nodes 1 to N scale as $sin((\alpha)^{1/2}n)$ [see (9)], the injection signal at node p can be written as

$$I_{inj,p} = K_{dist} V_o V_{inj} \sin(\sqrt{\alpha}p) \tag{17}$$

where K_{dist} is the mixing coefficient of the injection devices in the distributed injection-locked frequency divider. To have a fair comparison between the conventional injection-locked frequency divider of Fig. 1(a) and the proposed distributed injection-locked frequency divider of Fig. 3, we make the following assumptions.

1) Both schemes have the same impedance at the first parallel resonance frequency. This ensures that with the same current consumption, the two schemes will have the same self-oscillation frequency and voltage swing.
2) The switches scale with the size of the capacitors at each node. This is particularly true in millimeter wave (mm-wave) implementations, where the parasitic capacitors of the switch are dominant and no explicit capacitors are used.

From these assumptions, we note that the injection devices used in the distributed implementation should be scaled according to (12). This means that

$$K_{dist} = \frac{K_{conv}}{\sum_{i=1}^{N} \sin^2(\frac{\pi}{2N}i)} \tag{18}$$

where K_{conv} is the mixing coefficient of the injection device used in the corresponding conventional injection-locked frequency divider.

The total short-circuit injection current due to all N injection switches can be written as

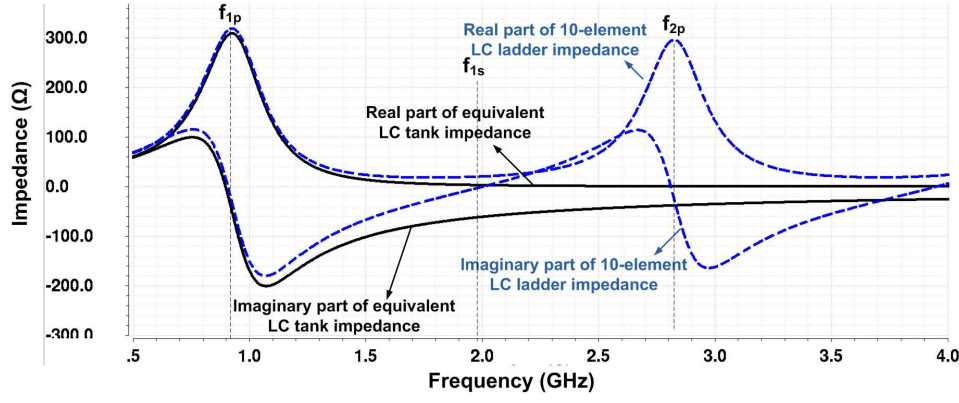$$I_{SC,dist} = \sum_{p=1}^{N} I_{SC,p} \tag{19}$$

Fig. 6. Simulated impedances of a ten-element LC-ladder and its equivalent LC tank of Fig. 5 ($L_1 = 1$ nH, $C_1 = 625$ fF, $R_1 = 18$ Ω, and $C_{eq} = 5.5C_1$).
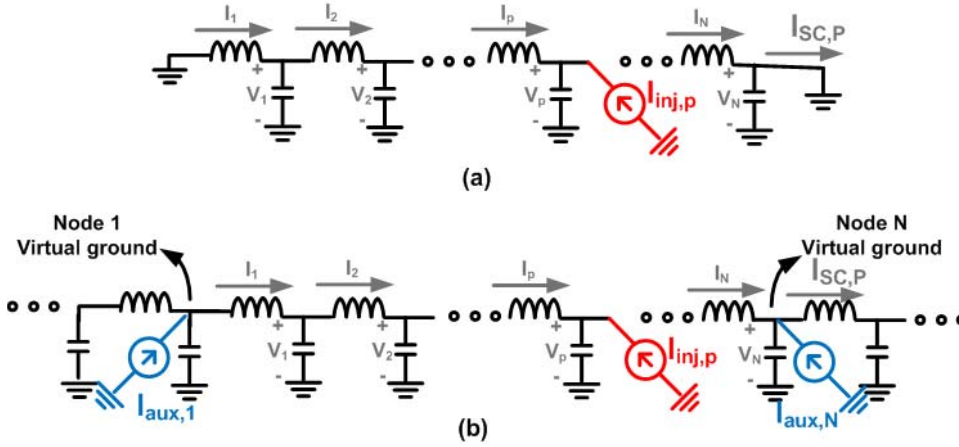

Fig. 7. (a) Short-circuit current from the pth injection in N-element LC-ladder. (b) Equivalent circuit based on double-sided ∞-element LC-ladder.
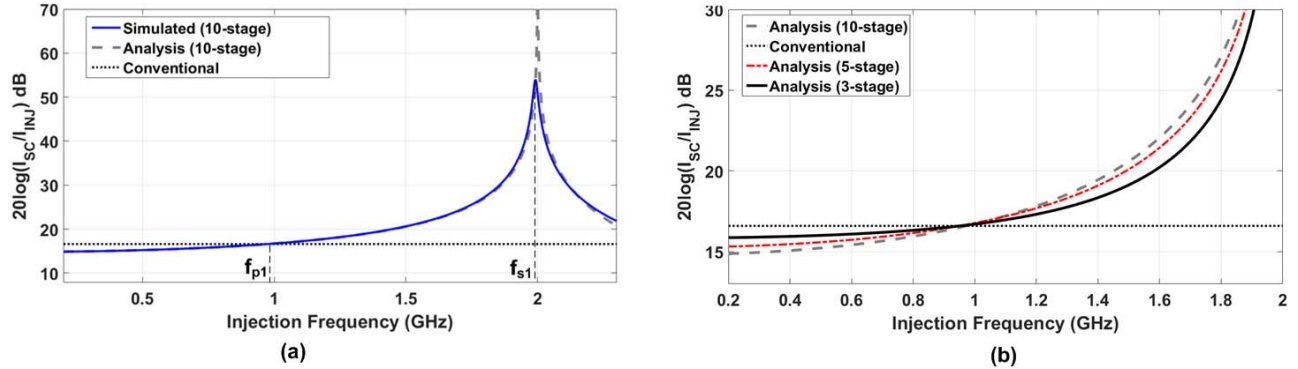

Fig. 8. (a) Analytical and simulated equivalent injection currents of a ten-element distributed and a conventional injection-locked frequency divider ($L_1 = 1$ nH, $C_1 = 625$ fF, $R_1 = 18$ Ω, and $C_{eq} = 5.5C_1$). (b) Comparison of injection strength of three-element, five-element, and ten-element distributed injection-locked frequency dividers.

that at ω_{1p}, from (16) and (17), simplifies to

$$I_{SC,dist}|_{@ \omega_{1p}} = \sum_{p=1}^{N} K_{dist} V_o V_{inj} \sin((\alpha)^{1/2} p)^2 = K_{conv} V_o V_{inj}. \tag{20}$$

This is a very interesting result; it states that in the proposed distributed injection-locked frequency divider, when the injection frequency is exactly double the first parallel resonance mode of the LC-network, the overall injection current due to

the scaled distributed injection devices will be equal to that of the single injection device in a conventional injection-locked frequency divider. However, unlike the conventional divider, the injection current in this distributed divider is frequency-dependent. Fig. 8(a) shows the total short-circuit equivalent injection current of a ten-element distributed injection-locked frequency divider as a function of frequency, below its first series mode resonance. The effective injection in the distributed scheme is weaker than that of the conventional frequency divider at frequencies below the first parallel resonance
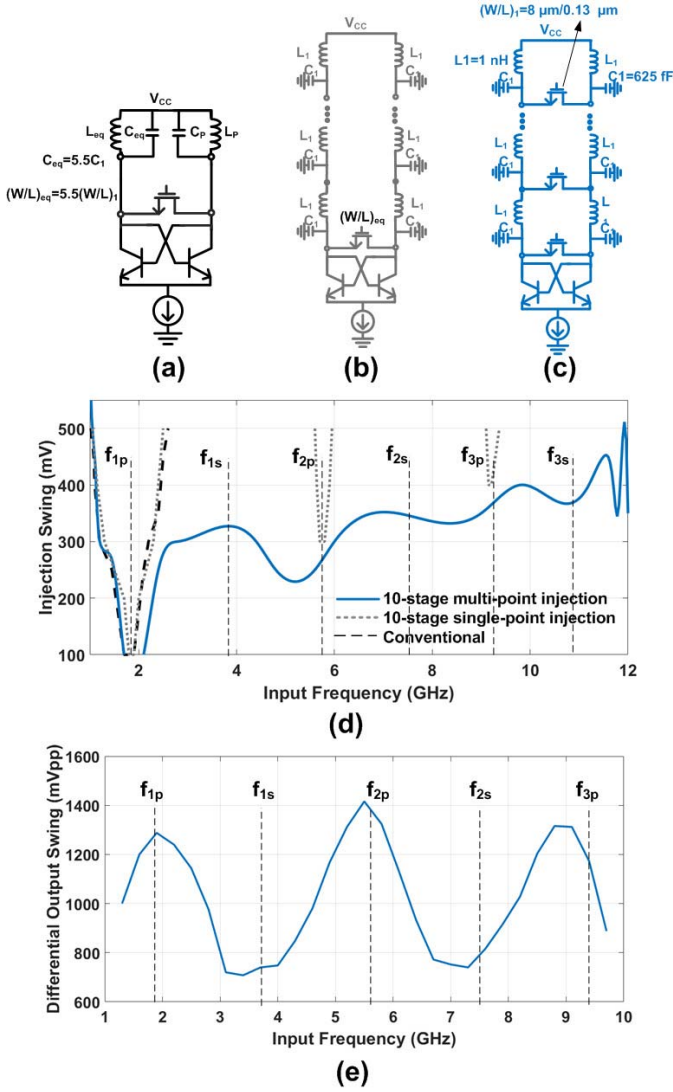
Fig. 9. (a) Conventional injection-locked frequency divider with *LC* load. (b) Injection-locked frequency divider with a distributed load. (c) Distributed injection-locked frequency divider. (d) Simulated sensitivity curves for the injection-locked frequency dividers of (a)–(c), where the *LC*-ladders consist of ten sections. (e) Simulated differential peak to peak swing across the cross-coupled pair in the ten-element distributed injection-locked frequency of (c) when $V_{\text{inj}} = 450\,mV$.

Fig. 10. Micrograph of the mm-wave distributed injection-locked frequency divider.

frequency and higher above that. Notice that the above-mentioned analysis will result in infinitely large injection at the series modes. Even after considering the finite quality factor of the network, the effective injection strength peaks at series modes and reduces to the same value in the parallel modes. It is also noteworthy that the increase in injection strength kicks in before reaching the 3-dB bandwidth of the series mode. Fig. 8(b) shows the comparison of the injection strength of a different number of elements. In this graph, the injection strength is normalized to the injection current of a conventional injection-locked frequency divider. The increase in injection strength beyond f_{p1} and below f_{s1} is negligible for a number of stages beyond 5. The injection strength will naturally be quite different at higher frequencies as the N-element ladder will have N parallel-mode resonances.
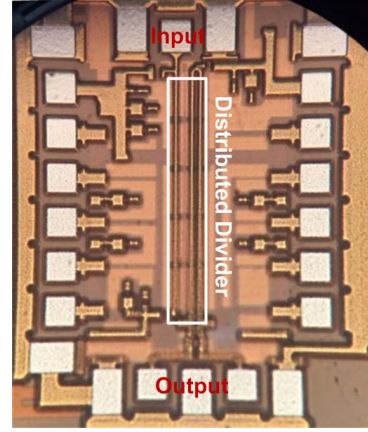
Because of this property of injection strength in the distributed injection-locked frequency divider, both gain and phase conditions can be satisfied for all parallel and series mode resonance frequencies. If designed properly, the frequency divider can operate continuously as a divide by 2 over multiples of the first resonance frequency. To the best of our knowledge, this is a property that has not been shown in any other injection-locked frequency divider. To illustrate this, consider three schematics shown in Fig. 9. Fig. 9(a) and (c) corresponds to a conventional and a distributed injection-locked frequency divider. Fig. 9(b) shows an alternate injection-locked frequency divider that has an *LC*-ladder distributed load, but only one injection device across the active core (similar to the conventional scheme). The *LC*-ladders in both Fig. 9(b) and (c) have all the parallel and series mode resonances. However, the equivalent injection current in the divider of Fig. 9(b) is frequency-independent and equal to that of the conventional design. Fig. 9(d) shows the simulated sensitivity curves of these three schematics. The distributed load/single point injection frequency divider of Fig. 9(b) can operate only around the parallel resonance frequencies and fails to divide at series resonance frequencies. In fact, in the absence of injection, startup condition is not satisfied at series mode resonances. This can be verified by comparing the negative conductance of the cross-coupled pair ($\approx -30\,mA/V$) to the conductance of the injection device plus the distributed load ($\approx 50\,mA/V$). As shown in Fig. 8, for ten-element distributed injection, the strength of injection is approximately 37 dB (effective gain of 70) higher in the first series resonance frequency compared with that of the first parallel resonance frequency. In Section II, we showed that for a normally ON injection device, injection helps the startup condition [see (4)]. Injection signal can satisfy the startup condition in spite of the low resistance of the load because of the large effective gain provided by the distributed network. Therefore, oscillation at half the injection frequency can be sustained at the series resonance frequency. The amplitude is limited by the fact that as the swing increases, the effective R_{ON} of the injection devices drops. As shown in Fig. 9(d), the distributed injection-locked frequency divider can divide continuously
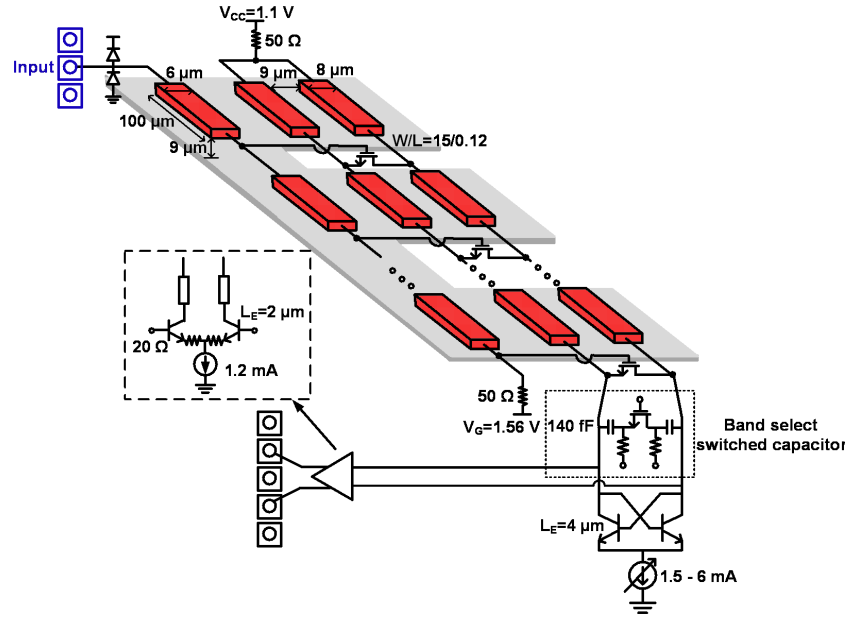
Fig. 11.   Schematics of the fabricated mm-wave distributed injection locked frequency divider with optimum bias conditions.
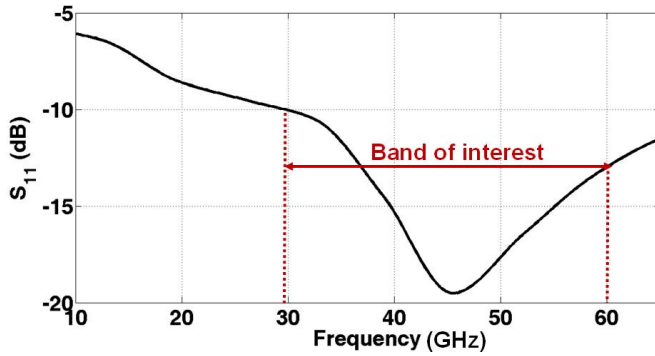

Fig. 12.   Measured reflection coefficient of the implemented distributed injection-locked frequency divider.
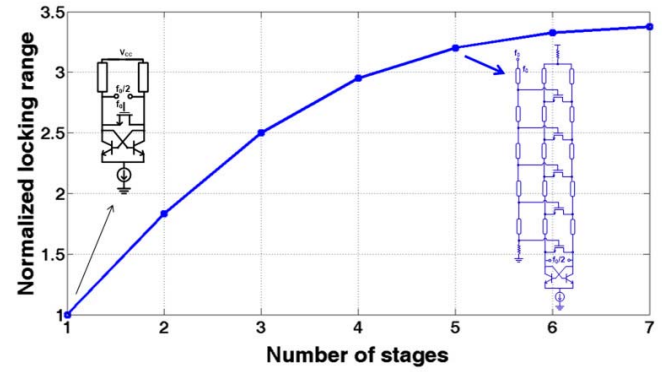

Fig. 13.   Simulated locking range of injection locked frequency dividers with different number of elements.

across multiple parallel and series resonance frequencies. This is due to the natural injection equalization in this scheme: as the impedance of the load drops, the injection strength increases. Notice that as one moves from parallel resonance frequencies toward series resonance frequencies, the injection strength increases, which helps satisfy the phase condition over a wider range [see (3)]. Fig. 9(e) shows the output swing of the ten-element distributed injection-locked frequency divider versus the injection frequency. Even though the self-oscillation condition is not satisfied at the series resonance modes, output amplitude at the first series resonance frequency is larger than half that of the first parallel mode resonance frequency.

It should be noted that from the presented first-order analysis, one might expect that the locking range of the distributed injection-locked divider will be smaller below the first parallel resonance frequency because of weaker injection (Fig. 8), but simulations show very similar behavior at the lower frequency end. This may be due to the very small difference in the effective injection strength between the two cases (below the first parallel resonance).
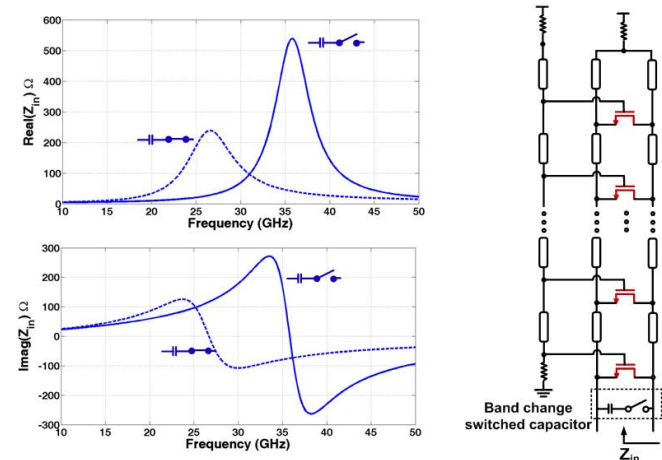

Fig. 14.   Simulation of impedance change due to switched capacitor close to the first parallel mode resonance frequency.

As a design example, consider a case where maximum input frequency of interest is 60 GHz and locking range is to be maximized. For a five-stage design, the first parallel mode
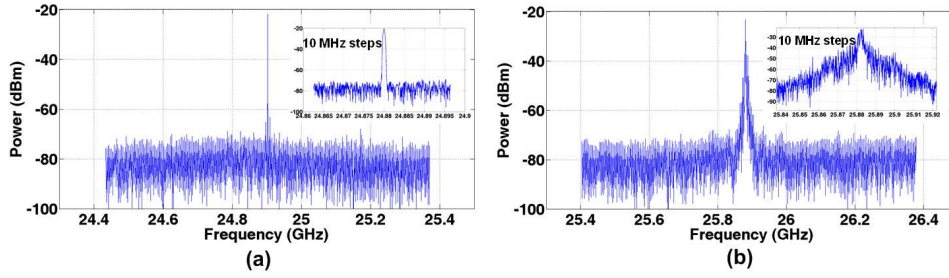
Fig. 15.　Measured (a) locked and (b) free-running (self-oscillation) output frequency spectrums.
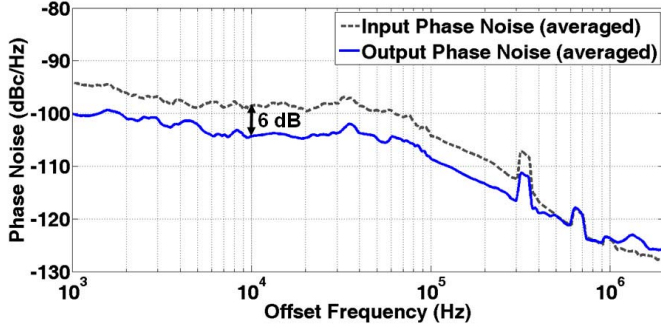

Fig. 16.　Measured phase noise of input (48 GHz) and output signals of the implemented distributed injection-locked frequency divider.
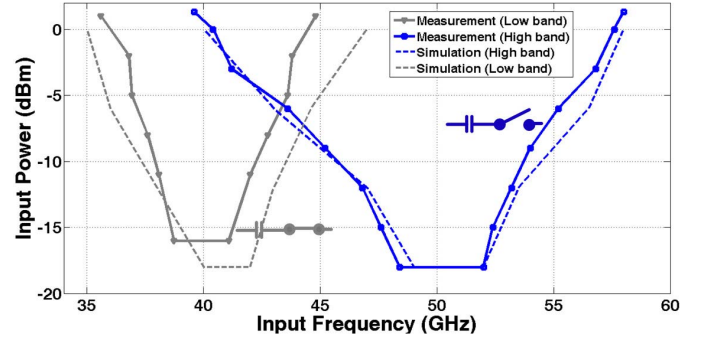

Fig. 17.　Simulated and measured sensitivity curves for high and low bands for nominal bias conditions.

Fig. 18.　Measured sensitivity curves for high dc current (phase condition limited).

resonance can be chosen at 6 GHz. This way, the fifth parallel mode of the resonator lies at 30 GHz (60 GHz/2). For a given current consumption, as discussed in this section, the required reactance of the core at 6 GHz is set (needs to resonate with the device parasitic capacitance). So, $L_1 C_1$ is set from (11). To determine the individual values of L_1 and C_1 (and hence the injection device switch size, assuming all of C_1 comes from the injection device), a more complicated optimization procedure is required. The concepts presented in Section II-A and II-B help significantly. In short: from (15) to (19) and the appendix, one can find the effective injection current as a function of injection frequency and injection device size. Given the injection strength and the negative conductance of the active core, the minimum injection device size to satisfy gain condition can be found (refer to discussions on gain condition in Section II-A). The device size should be increased as long as the R_{ON} of the injection device start to dominate the gain condition. At this point, the size of the injection device and the value for L_1 are determined and a first cut design is achieved.

III. IMPLEMENTATION OF AN MM-WAVE DISTRIBUTED INJECTION-LOCKED FREQUENCY DIVIDER

As shown in Section II-B, distributed injection locking technique can be used to improve the locking range beyond the conventional limits of injection-locked frequency dividers. An mm-wave implementation of the proposed scheme is discussed in this section [11]. Fig. 10 shows the micrograph of the chip. The chip has an area of $1\ mm \times 0.9\ mm$ and is fabricated in the IBM 0.13-μm SiGe BiCMOS technology (8HP). The divider's active area is 630 μm × 90 μm as marked in Fig. 10.

Fig. 11 shows the complete schematics of the fabricated chip. The cross-coupled active core of the divider uses 4-μm emitter length HBT bipolar transistors nominally biased at current density of $I_C / L_E = 0.5\ mA/\mu$m, which results in close-to maximum effective negative conductance at the frequency of interest. The total capacitance of the device (100 fF differential) and the required self-oscillation frequency determined by the band of interest sets the required reactance of the distributed load. The implementation is a five-stage design where microstrip transmission lines are used to implement the inductors. In this technology, three thick metal layers may be used to implement the transmission lines. The top and bottom thick metal layers are chosen for the signal and ground layer of the transmission lines to maximize inductor per length while reducing loss. Each element transmission line (100 μm length) amounts to 50-pH inductance with Q = 12 at the center

TABLE I
COMPARISON WITH mm-WAVE FREQUENCY DIVIDERS

|	Technology	Opration Frequency (GHz)	Locking Range	Power Consumption (mW)	Core Area (mm²)	Topology
This Work	0.13 μm BiCMOS	35 - 44 41 - 59.5	Low band: 22% High band: 37% Total: 53%	3.8	0.046	Distributed Injection Locking (IL)
[7]	32 nm CMOS	40 - 70	54%	4.8	0.001	Dynamic latch with load modulation
[2]	65 nm CMOS	53.4 - 79	39%	2.9	0.126	Freq. Track IL
[4]	65 nm CMOS	48.5 - 62.9	25.9%	1.65	0.015	Multi-order tank IL
[5]	0.13 μm CMOS	59.6 - 67	11.6%	1.6	0.017	Class-B IL
[6]	0.18 μm CMOS	37.5 - 49	26.6%	6	0.428	regenerative
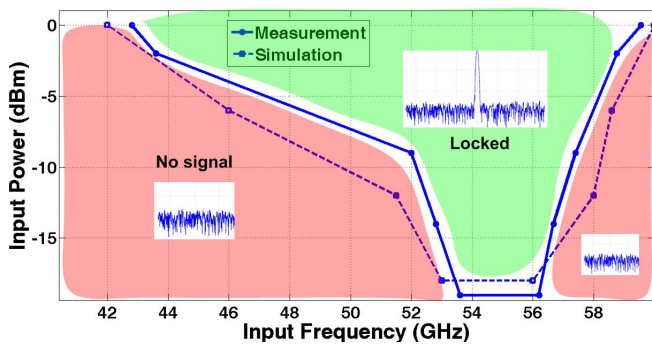
Fig. 19. Measured sensitivity curves for low dc current (gain condition limited).

frequency. Five microstrip transmission lines are used for the input feed and coupled differential transmission lines are used for the core distributed resonator. The 55-pH inductance per element at the input feed and the 20-fF gate capacitance and interconnect parasitics result in close to 50-Ω characteristic impedance for the quasi-distributed input transmission line. The parasitics of the input electro-static discharge diode and the injection NMOS devices are incorporated into the input artificial transmission line network, preventing them from limiting the input matching bandwidth. Fig. 12 shows the reflection coefficient measurement of the input network. In this implementation, the maximum oscillation frequency of the cross-coupled pair consisting of two 4 μm emitter length transistors is 65 GHz. Because of this limitation, gain condition cannot be satisfied at higher order resonance modes. However, the significantly improved injection strength beyond the self-oscillation frequency of the divider results in a wide locking range (Fig. 13).

An additional switched MIM capacitor is added across the cross-coupled pair to extend the division frequency to lower frequencies by reducing the self-oscillation frequency of the divider. Fig. 14 shows the simulated impedance of the ladder network for both states of the switched capacitor. The buffer is an open-collector differential pair with resistive degeneration to reduce the capacitive loading of the buffer on the divider core. Fig. 15 shows representative spectrum measurements of

the output signal read directly from the spectrum analyzer when the MIM capacitor is not switched in. For nominal bias conditions ($V_G = 1.6$ V, $V_{CC} = 1.2$ V $I_{core} = 4$ mA, and $I_{buf} = 1.5$ mA), the self-oscillation frequency for the high and low bands is 25.9 and 21.3 GHz, respectively. An alternative design could use a load with a smaller first parallel mode resonance frequency to cover a wider range (e.g., 10–60 GHz). The output power for nominal bias conditions is measured at −21 dBm single-ended (simulated −19 dBm), and is −25 dBm for the low band. Fig. 16 shows the measured phase noise of the input and divided output for a 48-GHz input signal with −10 dBm power. The phase noise at lower offsets follows the input phase noise with 6-dB difference (the standard deviation from the ideal divided phase noise from 1 kHz to 1 MHz is 0.73 dB). The phase noise floor beyond 1 MHz varies as the bias current of the buffer (and hence output power) is changed, indicating that it is the combined phase noise floor of the buffer and the measurement instrument.

Fig. 17 shows the simulated and measured sensitivity curves for nominal design bias conditions ($V_G = 1.6$ V, $V_{CC} = 1.2$ V, $I_{core} = 4$ mA, and $I_{buf} = 1.5$ mA). The spectrum beyond the sensitivity curve region shows the characteristics of a pulled oscillator spectrum, indicating that locking is lost by not satisfying the phase condition. As expected from the previous analysis, the achieved locking range is varied as the bias conditions (e.g., gate–source voltage of injection devices, active core, and buffer bias current) are changed. When changing the bias conditions, two separate regimes of operation are observed. Fig. 18 shows sensitivity curves for $I_{core} = 5$ mA and $I_{buf} = 0.9$ mA. Since the effective transconductance of the cross-coupled pair guarantees startup condition, the injection-locked divider only shows frequency pulling outside the locking range. Below 2.8 mA, at the edge of the locking range, the output signal disappears, indicating that the gain condition is not satisfied due to injection devices loss. An example sensitivity curve is shown in Fig. 19 for $I_{core} = 2.5$ mA and $I_{buf} = 0.6$ mA. For $V_G = 1.54$ V, $V_{CC} = 1.1$ V, $I_{core} = 3.5$ mA, and $I_{buf} = 0.9$ mA, maximum locking range of 41–59.5 GHz for the high band and 35–44 GHz for the low band for 0-dBm input power is achieved. Table I shows the performance in comparison with

selected published mm-wave frequency dividers. It should be noted that the injection switches in this design are 0.13-μm CMOS transistors, and migrating to a lower CMOS node is expected to improve the locking range even further due to increase in injection strength (K') for the same parasitic capacitance.

IV. CONCLUSION

In this paper, the concept of distributed injection-locked frequency division is introduced to increase the locking range beyond conventional limits of injection-locked frequency dividers. It is analytically shown that continuous frequency division can be achieved over a frequency range that spans over multiples of the self-oscillation frequency of the core divider. As a proof-of-concept, a prototype was realized in a foundry 130-nm BiCMOS SiGe HBT technology, achieving a measured locking range of 35–44 and 41–59.5 GHz while consuming 3.8 mW from a 1.15-V supply.

APPENDIX

A. Injection Switch Model

In general, the current of the MOS injection device shown in Fig. 1(b) is a complicated nonlinear function of the injection signal and the core signal as the switch goes through different operating regions (OFF, triode, saturation, velocity saturation, and so on). In this appendix, we will simplify this function to the point where it leads to accurate predictions of the injection-locked divider while the analysis remains simple enough to draw intuitive conclusions about the dynamics of the divider. Similar to (1), for the switch shown in Fig. 1(b), we define

$$\begin{cases} V_{od0} = V_G - V_{CC} - V_{th0} \\ \Theta_{inj} = \omega_{inj}t \\ \Theta_o = \omega_0 t + \phi(t) \end{cases} \quad (21)$$

where V_{od0} is the switch dc overdrive voltage, and Θ_{inj} and Θ_o represent the time varying phase arguments of the injection and output voltage waveforms. The injection device current corresponding to cutoff, triode, and moderate saturation is given by

$$I_{SW} = \begin{cases} 0, \\ \quad V_{inj}\cos\Theta_{inj} + V_o|\cos\Theta_o| + V_{od0} < 0 \\ K'(V_{inj}\cos\Theta_{inj}+V_o|\cos\Theta_o|+V_{od0})2V_o\cos\Theta_o, \\ \quad V_{inj}\cos\Theta_{inj} - V_o|\cos\Theta_o| + V_{od0} > 0 \\ K'(V_{inj}\cos\Theta_{inj}+V_o|\cos\Theta_o|+V_{od0})^2 sgn(\cos\Theta_o), \\ \quad \text{otherwise} \end{cases} \quad (22)$$

where sgn(.) is the sign function with the value of $+1(-1)$ when the argument is more (less) than zero. We have ignored velocity saturation. For the two cases of triode and moderate saturation, considering only the terms that

have frequency components close to the resonator frequency (ω_o), the injection device current may be simplified as

$$I_{SW} \approx 2K'V_{inj}V_o\cos\Theta_{inj}\cos\Theta_o + 2K'V_{od0}V_o\cos\Theta_o. \quad (23)$$

Therefore, the injection device current throughout the entire cycle may be written as

$$I_{SW} = \begin{cases} 0, & V_{inj}\cos\Theta_{inj} \\ \quad + V_o|\cos\Theta_o| + V_{od0} < 0 \\ 2K'V_{inj}V_o\cos\Theta_{inj}\cos\Theta_o \\ \quad + 2K'V_{od0}V_o\cos\Theta_o, & \text{otherwise.} \end{cases} \quad (24)$$

B. LC-Ladder Analysis

From (8), the equation for inductor currents may be written as

$$I_{k+1} - I_k = -\alpha \sum_{m=1}^{k} I_m \quad (25)$$

where $\alpha = L_1 C_1 \omega^2$. The difference equation for inductor current may be written as

$$I_k - (2-\alpha)I_{k-1} + I_{k-2} = 0. \quad (26)$$

The poles of the one-sided z-transform of the difference equation are given by

$$z^{-1} = \frac{2 - \alpha \pm \sqrt{\alpha^2 - 4\alpha}}{2}. \quad (27)$$

For small α, the poles can be approximated as $z^{-1} \approx 1 - \frac{\alpha}{2} \pm j(\alpha)^{1/2}$. Equation (9) can then be derived by taking the inverse z-transform and applying the boundary conditions.

REFERENCES

[1] J. Yin and H. C. Luong, "A 57.5–90.1-GHz magnetically tuned multimode CMOS VCO," *IEEE J. Solid-State Circuits*, vol. 48, no. 8, pp. 1851–1861, Aug. 2013.

[2] Y. Chao and H. C. Luong, "Analysis and design of a 2.9-mW 53.4–79.4-GHz frequency-tracking injection-locked frequency divider in 65-nm CMOS," *IEEE J. Solid-State Circuits*, vol. 48, no. 10, pp. 2403–2418, Oct. 2013.

[3] B. Razavi, "A study of injection locking and pulling in oscillators," *IEEE J. Solid-State Circuits*, vol. 39, no. 9, pp. 1415–1424, Sep. 2004.

[4] K. Takatsu *et al.*, "A 60-GHz 1.65 mW 25.9% locking range multi-order LC oscillator based injection locked frequency divider in 65 nm CMOS," in *Proc. IEEE CICC*, 2010, pp. 1–4.

[5] R. Sujiang *et al.*, "0.9 mW 7 GHz and 1.6 mW 60 GHz frequency dividers with locking-range enhancement in 0.13 μm CMOS," in *IEEE ISSCC Dig. Tech. Papers*, Sep. 2009, pp. 96–97.

[6] J. Chien and L. Lu, "40GHz wide-locking-range regenerative frequency divider and low-phase-noise balanced VCO in 0.18 μm CMOS," in *IEEE ISSCC Dig. Tech. Papers*, Sep. 2007, pp. 544–621.

[7] A. Ghilioni, A. Mazzanti, and F. Svelto, "Analysis and design of mm-Wave frequency dividers based on dynamic latches with load modulation," *IEEE J. Solid-State Circuits*, vol. 48, no. 8, pp. 1842–1850, Aug. 2013.

[8] A. Goel and H. Hashemi, "Injection locking in concurrent dual-frequency oscillators," *IEEE Trans. Microw. Theory Techn.*, vol. 56, no. 8, pp. 1834–1845, Aug. 2008.

[9] R. Adler, "A study of locking phenomena in oscillators," *Proc. IRE*, vol. 34, no. 6, pp. 351–357, Jun. 1946.

[10] R. M. Foster, "A reactance theorem," *Bell. Syst. Tech. J.*, vol. 3, no. 2, pp. 259–267, Apr. 1924.

[11] A. Imani and H. Hashemi, "A 3.9 mW, 35–44/41–59.5 GHz distributed injection locked frequency divider," in *Proc. IEEE CICC*, Sep. 2015, pp. 1–4.

Alireza Imani received the B.S. and M.S. degrees in electrical engineering (electronics) from the Sharif University of Technology, Tehran, Iran, in 2006 and 2008, respectively, and the Ph.D. degree in electrical engineering from the University of Southern California, Los Angeles, CA, USA, in 2016.

He joined Broadcom Limited as an RFIC Design Engineer in 2016. His current research interests include RF and mm-wave circuits and systems, including frequency generation, nonlinear dynamics, and phased arrays.

Dr. Imani was a recipient of the 2015 IEEE CICC Best Student Paper Award (first place). He was ranked first in the 2006 National Electrical Engineering Olympiad, Iran.

Hossein Hashemi (SM'08) received the B.S. and M.S. degrees in electronics engineering from the Sharif University of Technology, Tehran, Iran, in 1997 and 1999, respectively, and the M.S. and Ph.D. degrees in electrical engineering from the California Institute of Technology, Pasadena, CA, USA, in 2001 and 2003, respectively.

In 2003, he joined the Ming Hsieh Department of Electrical Engineering–Electrophysics, University of Southern California, Los Angeles, CA, USA, where he is currently a Professor, a Ming Hsieh Faculty Fellow, and the Co-Director of the Ming Hsieh Institute. He is the Co-Editor of the books *Millimeter-Wave Silicon Technology: 60 GHz and Beyond (Springer, 2008)* and *Millimeter-Wave Silicon Power Amplifiers and Transmitters* (Cambridge University Press, 2015). His current research interests include electrical and optical integrated systems.

Dr. Hashemi was a member of the Technical Program Committee of the IEEE International Solid-State Circuits Conference from 2011 to 2015 and the IEEE Compound Semiconductor Integrated Circuits Symposium from 2010 to 2014. He has been a member of the IEEE Radio Frequency Integrated Circuits Symposium since 2011. He was a co-recipient of the 2016 Nokia Bells Labs Prize. He was a recipient of the 2015 IEEE Microwave Theory and Techniques Society Outstanding Young Engineer Award, the 2008 Defense Advanced Research Projects Agency Young Faculty Award, the National Science Foundation Career Award, the USC Viterbi School of Engineering Junior Faculty Research Award in 2008, and was recognized as a Distinguished Scholar for Outstanding Achievement in Advancement of Engineering by the Association of Professors and Scholars of Iranian Heritage in 2011. He was a co-recipient of the 2004 JSSC the Best Paper Award for A Fully Integrated 24-GHz 8-Element Phased-Array Receiver in Silicon and the 2007 IEEE ISSCC Lewis Winner Award for Outstanding Paper for A Fully Integrated 24-GHz 4-Channel Phased-Array Transceiver in 0.13-?m CMOS based on a Variable Phase Ring Oscillator and PLL Architecture. He served as a Distinguished Lecturer of the IEEE Solid-State Circuits Society from 2013 to 2014. He was an Associate Editor of the IEEE TRANSACTIONS ON CIRCUITS AND SYSTEMS I from 2006 to 2007 and the IEEE TRANSACTIONS ON CIRCUITS AND SYSTEMS II from 2004 to 2005. He has been an Associate Editor of the IEEE JOURNAL OF SOLID-STATE CIRCUITS since 2013. He was a Guest Editor of the IEEE JOURNAL OF SOLID-STATE CIRCUITS in 2013.